Estuarine, Coastal and Shelf Science 294 (2023) 108525

Contents lists available at ScienceDirect

Estuarine, Coastal and Shelf Science

journal homepage: www.elsevier.com/locate/ecss

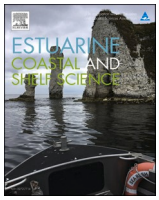

Two centuries of southwest Iceland annually-resolved marine temperature reconstructed from *Arctica islandica* shells

M.J. Mette [a,b,*], C. Andersson [b], B.R. Schöne [c], F.G.W. Bonitz [b], V. Melvik [b], T. Trofimova [b], M. W. Miles [b,d]

[a] U.S. Geological Survey, St. Petersburg Coastal and Marine Science Center, St. Petersburg, Florida, USA
[b] NORCE Norwegian Research Centre, Bjerknes Centre for Climate Research, Bergen, Norway
[c] Institute of Geosciences, University of Mainz, Mainz, Germany
[d] Institute of Arctic and Alpine Research, University of Colorado, Boulder, USA

ARTICLE INFO

Keywords:
Sclerochronology
North Atlantic Ocean circulation
Shell growth chronology
Temperature reconstruction
Oxygen isotopes

ABSTRACT

Iceland's exposure to major ocean current pathways of the central North Atlantic makes it a useful location for developing long-term proxy records of past marine climate. Such records provide more detailed understanding of the full range of past variability which is necessary to improve predictions of future changes. We constructed a 225-year (1791–2015 CE) master shell growth chronology from 29 shells of *Arctica islandica* collected at 100 m water depth in southwest Iceland (Faxaflói). The growth chronology provides a robust age model for shell oxygen isotope ($\delta^{18}O_{shell}$) data produced at annual resolution for 251 years (1765–2015 CE). The temperature reconstruction derived from $\delta^{18}O_{shell}$ shows coherence with May–October local surface temperature records and sea surface temperatures in the North Atlantic region, suggesting it is a useful proxy indicator of water temperature variability at 100 m depth within Faxaflói. Field correlations between the shell-based records and gridded sea surface temperature data reveal strong positive correlations between the 1-year lagged shell growth and temperatures within the subpolar gyre post-1972, suggesting a delayed influence of subpolar gyre dynamics on ecological indicators in southwest Iceland in recent decades. However, the shell growth chronology and $\delta^{18}O_{shell}$ record generally show relatively weak and insignificant correlations with larger region climate indices including the Atlantic Multidecadal Variability, North Atlantic Oscillation, and East Atlantic pattern. Therefore the interannual variations in the newly produced shell-based records appear to reflect more local to regional dynamics around southwest Iceland than large-scale modes of climate variability.

1. Introduction

North Atlantic Ocean dynamics are important drivers of global climate, yet the complexities among major current systems, large-scale teleconnections, and ocean-atmosphere exchanges pose significant challenges for understanding and modeling past and future change. Uncertainty and debate exist about, for example, the past and predicted behavior of the Atlantic Meridional Overturning Circulation (AMOC; Caesar et al., 2021), the role of surface ocean circulation dynamics in past local to regional climate events (Lund et al., 2006), and the nature and impacts of large-scale low-frequency modes such as Atlantic Multidecadal Variability (AMV; Zhang et al., 2019). Long-term records of hydrographic variability are important for reaching a more comprehensive understanding of marine climate of the North Atlantic Ocean. Due to limited length of instrumental records, development of geographically diverse, multicentury proxy reconstructions of hydrographic variability is necessary. Its exposure to major ocean current pathways of the central North Atlantic (Fig. 1) makes Iceland a key locality for developing long-term proxy records of marine climate to understand the full range of past variability and provide context for present and future changes.

Shells from the marine bivalve *Arctica islandica* have increasingly been applied as environmental proxy archives across the northern North Atlantic over the past few decades (Schöne, 2013). Records from shells of *A. islandica* are used in paleoclimate research as the marine equivalent to terrestrial records from trees (Fig. 2). Annual banding within the shell, synchronous growth rates within populations, and the long lifespan of individuals (maximum >500 years; Butler et al., 2013) enable

* Corresponding author. U.S. Geological Survey, St. Petersburg Coastal and Marine Science Center, St. Petersburg, Florida, USA.
E-mail address: mmette@usgs.gov (M.J. Mette).

https://doi.org/10.1016/j.ecss.2023.108525
Received 6 April 2023; Received in revised form 31 August 2023; Accepted 6 October 2023
Available online 21 October 2023

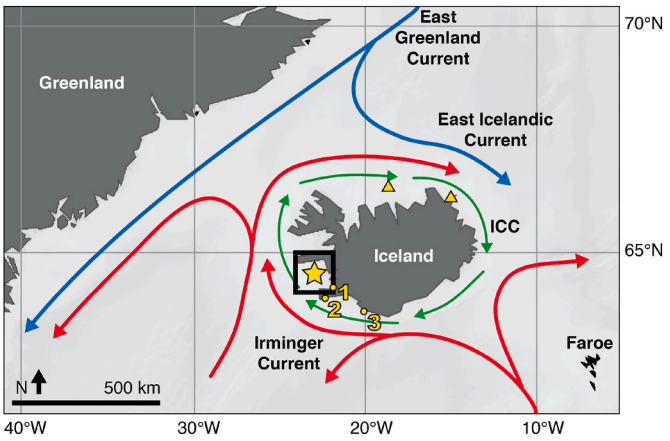

Fig. 1. Map showing shell collection site (yellow star) and ocean currents surrounding Iceland (ICC = Iceland Coastal Current). Gridded sea surface temperatures used for analysis were extracted from the region encompassing Faxaflói (open square; 64–65°N, 22–24°W). Yellow triangles mark additional *Arctica islandica*-based records from Butler et al. (2013) and Reynolds et al. (2016) on the North Icelandic shelf, and Lohmann and Schöne (2013) off northeast Iceland. Nearby station-based sea surface temperature records are (1) Reykjavík, (2) Grindavík, and (3) Stórhöfði/Vestmannaejar. (For interpretation of the references to color in this figure legend, the reader is referred to the Web version of this article.)

the construction of lengthy (often multicentury) master shell growth increment width chronologies that are precisely dated (Butler et al., 2013; Black et al., 2019). The oxygen isotope composition of the aragonite shell material ($\delta^{18}O_{shell}$) provides a robust and commonly applied proxy for hydrographic variability (Weidman and Jones, 1994; Schöne, 2013; Reynolds et al., 2016). $\delta^{18}O_{shell}$ is controlled by the temperature and oxygen isotope composition of the water ($\delta^{18}O_{water}$) in which the shell is precipitated (Epstein et al., 1953).

The Iceland region is host to several study sites that have been used in the growing network of proxy records from *A. islandica* (Reynolds et al., 2018) and highly temporally resolved records from other archives (e.g., sediment cores, see Moffa-Sánchez et al., 2019) to study past North Atlantic Ocean dynamics. A radiocarbon reservoir age reconstruction using *A. islandica* from northwest Iceland suggests the Little Ice Age (LIA; approximately 1400–1850, or decades later in this region) was amplified by decreased flow of North Atlantic water south of Iceland (Wanamaker et al., 2012). Annual shell growth rate and $\delta^{18}O_{shell}$ records from the same population demonstrated how ocean circulation has played a role in modulating the response of North Atlantic climate to solar and volcanic forcing over the past millennium (Butler et al., 2013; Reynolds et al., 2016). *A. islandica* records from northeast Iceland have been used to explore proxy fidelity and multidecadal variability in the region's sea surface temperatures (SST) (Lohmann and Schöne, 2013; Marali and Schöne, 2015). Despite abundant *A. islandica* shell material in the southwest of Iceland within the embayment known as Faxaflói, shell-based proxy records have yet to be developed from this area. Such data would fill a geographical gap in records of marine climate variability around Iceland through the lens of the *A. islandica* proxy archive. The goal of this study is to assess the utility of *A. islandica* shell-based records from Faxaflói for reconstructing local to large-scale climate variability.

Our study presents newly developed, absolutely-dated, annually resolved, long-term records of shell growth, $\delta^{18}O_{shell}$, and an Atlantic Water temperature reconstruction using $\delta^{18}O_{shell}$ from *A. islandica* shells from Faxaflói. The exceptional age control of these records achieved via crossdating of shell growth increments (Black et al., 2019) provides high-quality data that complement existing proxy datasets in the region and contribute to a more complete understanding of local hydrographic variability around Iceland, as well as its larger-scale impacts. We explore the relationships between the shell-based records and marine and atmospheric modes measured over the instrumental period (primarily post-1950) in order to assess the degree to which the proxy data reflect the influence of larger-scale processes in the region. We present an overview of the statistical properties of the records and implications for future development and use of *A. islandica* shell growth and $\delta^{18}O_{shell}$ chronologies from Faxaflói.

2. Materials and methods

2.1. Sample collection and processing

Specimens (n = 29) of *A. islandica* came from the southwest Icelandic shelf in the Faxaflói area (Fig. 1) during two cruises on R/V *G.O. Sars* in July 2015 (GS15-198) and August 2016 (GS16-204). The shells were collected by dredging the seafloor using a custom-built rigid-toothed dredge from three different stations located within a 0.5 km^2 region at depths of approximately 100 m (see Table 1). Shells were harvested on board, open-air dried, and packaged for transport to the laboratory at NORCE Norwegian Research Centre, Bergen, Norway.

Shells were processed using standard sclerochronological procedures (e.g., Butler et al., 2009). A ~2 cm broad slab was cut along the axis of maximum growth from the left valve of each shell using a geological saw (Fig. 2a). Sections were labeled and embedded in Buehler EpoxiCure2 epoxy resin, allowed to cure, and bisected along the maximum growth axis using a Buehler IsoMet 5000 Linear Precision Saw. The mirror-image cross-sections were ground and polished using a Buehler

Table 1
Arctica islandica shell sampling locations in Faxaflói, SW Iceland.

Cruise	Station name	Water depth (m)	Latitude, Longitude
GS15-198	31	105	64° 22.01′ N, 23° 07.64′ W
GS15-198	23	103	64° 21.97′ N, 23° 07.45′ W
GS16-204	10	101	64° 21.54′ N, 23° 07.20′ W

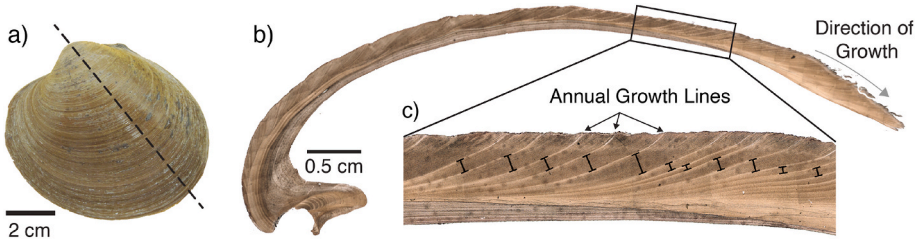

Fig. 2. *Arctica islandica* as a proxy archive. a) Left valve of a shell showing axis of maximum growth (dashed line) along which the specimen is bisected for further processing. b) Photomicrograph of an acetate peel replica of the polished shell cross-section. c) Magnified view of photomicrograph showing annual growth lines. The typical measurement axes for individual increments are superposed (black-capped lines). Reprinted with permission from "Persistent multidecadal variability since the 15th century in the Southern Barents Sea derived from annually resolved shell-based records" by M. J. Mette et al. (2021), *Journal of Geophysical Research: Oceans*, 126.

Phoenix Beta grinder polisher and silicon carbide grinding papers (up to 15 μm grit size). One section was etched in a 0.1 M HCl solution for 2–3 min. An acetate sheet (35 μm thickness; Agar Scientific) was applied over a thin layer of ethyl acetate onto the etched shell surface to produce acetate peel replicas of the shell cross-section. The acetate peels were mounted between glass microscope slides and photographed with an Infinity3 Lumenera camera mounted to a light compound microscope. Images and measurements were taken using ImagePro Premiere v9.1. Annual growth increments were measured perpendicular to the growth increment lines along the margin (Fig. 2b and c) and, in some cases, additionally along the hinge plate for comparison and assistance with crossdating. Original increment measurements were stored in proprietary measurement files (.iqm) and collated within a Microsoft Excel spreadsheet (see data availability statement).

2.2. Crossdating and chronology building

Growth increment crossdating and chronology construction followed standard techniques originating in the field of dendrochronology (Speer, 2010) and carried on in the field of sclerochronology (Black et al., 2019). Visual and statistical crossdating were performed to verify annual growth increment width series for 29 shells (Table 2). Visualization of running correlations between series using Shellcorr MatLab script version 5 b (Scourse et al., 2006) aided in locating potential errors in increment identification. Any flagged mismatch was verified through inspecting the shell material and images before correcting and updating the measurement series. Individual growth increment series were compiled in ARSTAN software version 44 (Cook, 1985; Cook et al., 2017). Between 5 and 22 of the first juvenile growth increments were excluded from each series where these earliest increments were too wide to measure perpendicular to the growth lines (Table 2). These increments also usually contain many "false" annual growth lines due to rapid juvenile growth and likely increased sensitivity to environmental disturbance. Therefore, the number of increments excluded from a series likely overestimates the number of years excluded from the series. Heteroscedasticity, i.e., the correlation between the local mean and variance was corrected for in each series by means of adaptive power transformation (Cook and Peters, 1997). To account for ontogenetic (age-related) growth trends not related to climate or environmental variability, each growth series was detrended using a Hugershoff growth function, which allows additional flexibility for more juvenile increments (as compared to less flexibility with a more typically applied negative exponential function; see Fang et al., 2010 and Butler et al., 2010 for more complete discussions of detrending). ARSTAN calculates a normalized growth index from the resulting detrended series to produce the master shell growth chronology (MSC), presented as a growth index (GI). The expressed population signal (EPS; Wigley et al., 1984) was calculated over 30-year windows with a 29-year overlap.

2.3. $\delta^{18}O$ sampling and analysis

Sub-annual $\delta^{18}O_{shell}$ sampling was performed in the inner portion of the outer shell layer along the margin of three live-collected juvenile shells over five annual growth increments representing the years 2005–2009. Two methods were used. In the first method, samples were drilled using a handheld industrial drill (Minimo One Series, V. 2, Minitor Co., Ltd) with conical drill bit (300 μm diameter at the tip; Komet/Gebr. Brasseler GmbH and Co., model H52 104 003). Sampling was performed at approximately equidistant intervals along the main growth axis of the shell margin. The first sample was taken adjacent to the annual growth line (the thin band of darker shell material marking the boundary between two annual increments). The final sample from each year was taken along the annual growth line to include the material produced at the boundary between two years. The second method used a Merchantek micromill with a 100 μm diameter mill bit (Komet/Gebr. Brasseler GmbH and Co. model no. H99 500 104 162 384 008). Ten

Table 2
Summary of shells included in the Master Shell Growth Chronology. Excluded increments represents juvenile growth increments that were measured but not crossdated (see text for discussion). Crossdating corrections indicates how many corrections were made during the crossdating process where increments were either falsely identified or missed by the technician at first pass. *The first year in series extends before 1770 for the first two shells listed, however, these earlier years were not used for chronology construction.

Shell ID	First year in series	Last year in series	Length of series	Excluded increments	Crossdating corrections (false/missed)
GS15-31-5	1770*	2014	244	8	5/11
GS16-7-3	1770*	2014	244	14	7/1
GS15-23-2	1791	2014	223	19	3/1
GS15-31-1	1792	2014	222	10	12/0
GS16-7-21	1793	2014	221	11	15/1
GS16-10-3	1819	2015	196	12	7/2
GS16-7-4	1836	2015	179	9	12/0
GS15-31-57	1839	2014	175	8	2/0
GS15-23-6	1875	2014	139	16	4/2
GS16-7-2	1875	2015	140	12	6/0
GS15-31-9	1878	2014	136	14	2/0
GS15-31-8	1892	2014	122	19	3/3
GS15-23-4	1893	2014	121	18	5/3
GS16-10-7	1896	2015	119	18	1/1
GS15-31-25	1897	2007	110	17	3/1
GS15-23-1	1904	2014	110	16	3/3
GS15-31-13	1916	2014	98	12	4/2
GS15-31-52	1920	2014	94	18	3/0
GS15-31-6	1936	2011	75	7	5/0
GS15-31-4	1937	2014	77	12	3/0
GS15-31-10	1938	2014	76	9	3/1
GS15-31-17	1944	2014	70	20	2/1
GS15-31-16	1945	2014	69	22	6/1
GS15-31-59	1958	2014	56	16	2/0
GS15-31-20	1963	2014	51	7	3/0
GS15-31-47	1963	2014	51	9	1/1
GS15-31-41	1964	2014	50	16	1/0

(continued on next page)

Table 2 (*continued*)

Shell ID	First year in series	Last year in series	Length of series	Excluded increments	Crossdating corrections (false/missed)
GS15-31-37	1966	2014	48	10	0/0
GS15-31-35	1979	2014	35	17	0/0

samples were taken per annual increment, with spacing determined by the total increment width and, thus, was variable between years. The first and final samples were both taken adjacent to the increment line, such that neither sample encompassed the entirety of the thin band (or growth line) that marks the boundary between two years (in contrast to the first method). The total depth milled into the cross section varied depending on the growth increment width and ranged between 20 μm (for wider increments) and 400 μm (for narrower increments) in order to obtain the required sample size for geochemical analysis (40–120 μg).

Annual $\delta^{18}O_{shell}$ sampling was performed in the outer margin of five crossdated shells with overlapping lifespans (four live-collected and one dead-collected) spanning the time interval 1765–2015 CE. Years sampled prior to 1791 CE were collected from a portion of a shell which was not crossdated (due to too few shells available in this time interval). Powdered samples were taken using the Merchantek micromill (same as above). The total depth milled into the cross-section for annual sampling varied between 200 μm (for broader increments) and 800 μm (for narrower increments). The annually resolved $\delta^{18}O_{shell}$ data used for analysis represent arithmetic averages across replicates where two or more shells were sampled.

Powdered shell samples (ca. 40–120 μg) were analyzed for $\delta^{18}O$ using a Thermo Fisher MAT 253 continuous-flow isotope ratio mass spectrometer equipped with a GasBench II at the Institute of Geosciences at the University of Mainz, Germany. Carbonate samples were digested in 10 mL He-flushed borosilicate exetainers at 72 °C using water-free phosphoric acid; reaction time was 2 h. Oxygen isotope data were then calibrated against an in-house Carrara marble standard (distributed by IVA Analysentechnik GmbH & Co. KG) with a value of −1.91 ‰. The long-term external precision (1σ) of the measurements was better than ±0.06 ‰ for $\delta^{18}O$, based on blind measurements of NBS-19 as well as IAEA-603. Individual samples with an internal precision ≥0.15 ‰ were excluded from further analysis. $\delta^{18}O_{shell}$ data are reported relative to the Vienna Peedee Belemnite (VPDB). Note that no correction was applied for differences in acid fractionation factors of the calcitic reference material and the shell aragonite because we used a paleothermometry equation (Eq. 1) that also did not account for these differences (further details are given in Füllenbach et al., 2015).

Water temperature was estimated from $\delta^{18}O_{shell}$ values using the aragonite-temperature equation of Grossman and Ku (1986) with a scale correction by Dettman et al. (1999) (Eq. (1)). A value of −0.07 $‰_{VSMOW}$ was used for the isotopic composition of water ($\delta^{18}O_{water}$), estimated from a simple mean of measurements taken from surface water in the harbor region in the NE of the city of Reykjavík between October 2010 and May 2012 (Table 3). We apply a constant value of $\delta^{18}O_{water} = -0.07$ $‰_{VSMOW}$ for all reconstructed $\delta^{18}O_{shell}$-based temperature estimates due to the low year-to-year salinity variation observed from station data at 100 m near the study site between the years 1947–2018 (2σ standard deviation = 0.11; see Section 2.4 for description of data source). For the oxygen isotope analysis of water, ca. 500 μl was transferred to He–CO_2-flushed exetainers and allowed to equilibrate at room temperature for 24 h. Then, the samples were measured on the equipment described above at the University of Mainz, and data were calibrated against V-GISP, V-SMOW and V-SLAB.

$$T\ (°C) = 20.60–4.34 \times (\delta^{18}O_{shell} - (\delta^{18}O_{water} - 0.27)) \quad \text{(Eq. 1)}$$

Table 3
Oxygen isotope composition of seawater samples ($\delta^{18}O_{water}$) taken from the harbor region (ca. 15 cm water depth) in the northeast of the city of Reykjavík between October 2010 and May 2012. Samples Ryk1 to 10 came from approximately 64°09′08.10″N, 021°57′29.53″W, and Ryk14 and 15 from 64°07′52.32″N, 021°57′38.35″W.

Sample ID	$\delta^{18}O_{water}$ ($‰_{VSMOW}$)
Ryk1-21.10.2010	0.22
Ryk1-21.10.2010	0.27
Ryk2-09.11.2010	−0.27
Ryk2-09.11.2010	−0.15
Ryk4-17.01.2011	−0.78
Ryk4-17.01.2011	−0.61
Ryk4-17.01.2011	−0.70
Ryk5-15.02.2011	−0.05
Ryk5-15.02.2011	0.08
Ryk5-15.02.2011	0.08
Ryk5-15.02.2011	0.03
Ryk6-08.03.2011	−0.16
Ryk6-08.03.2011	0.01
Ryk6-08.03.2011	−0.05
Ryk6-08.03.2011	−0.04
Ryk7-27.03.2011	−0.49
Ryk7-27.03.2011	−0.30
Ryk7-27.03.2011	−0.36
Ryk7-27.03.2011	−0.31
Ryk8-19.04.2011	0.00
Ryk8-19.04.2011	0.09
Ryk8-19.04.2011	0.16
Ryk8-19.04.2011	0.09
Ryk9-03.05.2011	0.09
Ryk9-03.05.2011	0.18
Ryk9-03.05.2011	0.21
Ryk9-03.05.2011	0.18
Ryk10–13.05.2011	0.01
Ryk10–13.05.2011	0.09
Ryk10–13.05.2011	0.17
Ryk10–13.05.2011	0.13
Ryk14 19Apr12	−0.05
Ryk15 21May12	−0.07

Estimated combined uncertainty (1.47 °C) for reconstructed temperatures is calculated as $\sqrt{(a^2+b^2)}$ and derived from uncertainty related to instrumental precision (a; 0.52 °C; 2-sigma standard deviation) and the Grossman and Ku (1986) temperature equation (b; 1.37 °C; mean squared error determined from the model fit to "mollusk-only" data available in Table 2 of Grossman and Ku, 1986; after Mette et al., 2018). Uncertainty related to $\delta^{18}O_{water}$ is not included in the combined uncertainty estimate due to a lack of data on $\delta^{18}O_{water}$ variability at 100 m depth near the study site. While we consider the mean $\delta^{18}O_{water}$ of surface waters (–0.07 $‰_{VSMOW}$, Table 3) to be a reasonable estimate for mean conditions at depth, we consider the variability in surface measurements to be greatly dampened, and acknowledge that our combined uncertainty is likely an underestimate.

2.4. Instrumental and proxy-based data for comparison

Local instrumental temperature measurements from the Icelandic Marine Research Institute (MRI; http://www.hafro.is/Sjora/; last access: November 2019) were used for determining the shell growing season and estimating the mean and variance of temperature and salinity nearest the collection site. These data comprise seasonally sampled temperature and salinity at 0–100 m depth from two stations along the Faxaflói standard line southwest of the sampling site, FX3 (18.7 km distance) and FX4 (23.2 km distance). Because these data are sparsely sampled (1–4 measurements per year), several strategies were used to compile the data to obtain useful summary statistics. A single time series at each depth category (0 m, 20 m, 50 m, 100 m) was created by averaging measurements taken within the same fortnightly period among both stations (usually n = 1 or n = 2). To visualize the seasonal

cycle not fully apparent using the one to nine measurements available in any one year, measurements taken from both stations were collated and averaged by day of year. Daily means were estimated from a local polynomial regression fit to these data performed in R (Version April 1, 1717; function "loess" with span set to 0.75) and averaged over periods of interest (e.g., May–Oct).

Long-term monthly SST measurement time series near Faxaflói were obtained from Trausti Jónsson at the Iceland Meteorological Office (Jónsson, 2003). These data are sampled at higher temporal resolution than the MRI data. Thus, time series of monthly and annual means are used for comparison with the annually resolved shell temperature reconstruction. Gridded monthly SST data derived from the Hadley Centre Sea Surface Temperature product (HadISST1 v1; Rayner et al., 2003) were also used for comparison. These data represent reanalyzed gridded SST from 1870–present and were extracted from a 2 × 4° grid box (averaged over 65–63°N to 24–20°W) within Faxaflói. Two versions of the AMV index using HadlSST (van Oldenborgh et al., 2009; Trenberth and Shea, 2006), two versions of the North Atlantic Oscillation (NAO) index (Jones et al., 1997; CPC), and the East Atlantic index (EA; CPC) were obtained from The Royal Netherlands Meteorological Institute's (KNMI) Climate Explorer web application (https://climexp.knmi.nl; downloaded 05/19/2021).

The *A. islandica* shell growth chronology (Reynolds et al., 2016) and $\delta^{18}O_{shell}$ record (Butler et al., 2013) from the North Icelandic Shelf were downloaded from https://www.ncei.noaa.gov/access/paleo-search/study/20448 and https://www.ncei.noaa.gov/access/paleo-search/study/14609, respectively (last access: November 2019). The *A. islandica* shell growth chronology off northeast Iceland was obtained from Lohmann and Schöne (2013; tabularized SGI data available at https://www.researchgate.net/publication/367334726_Lohmann_Schone_2013_PPP_373_152_sclero_Arctica_decadal_climate_var_Iceland_SLP_AMO_scleroxls; last access: Jan 22, 2023).

Comparisons were assessed using Pearson correlation coefficients (r) with a significance threshold of $p < 0.05$ (not adjusted for autocorrelation in the time series). Field correlation analyses were performed using KNMI Climate Explorer.

3. Results

3.1. Annual shell growth chronology

The master shell growth chronology (MSC; Fig. 3, bottom panel) comprises 28 live-collected shells and one dead-collected specimen. The 225-year record spans 1791−2015 CE with the number of included series at maximum from 1979–2007 (n shells = 29) and minimum in 1791 (n shells = 3). The expressed population signal (EPS), a measure of the common variability in a chronology that is dependent on sample depth, remains above 0.85 across the length of the chronology (Fig. 3, top panel) comprising three or more individual series, suggesting the record is suitable for environmental comparison (Wigley et al., 1984; Speer, 2010). Mean series length, a measure of the average length of series included in the chronology between 1791 and 2015, was 178 years. The longest- and shortest-lived shells included in the chronology were 427 and 36 years, respectively. The growth increment measurement series of the longest-lived specimen (shell ID: GS15-31-5SL) spanned 1588−2014. Because crossdating was only performed where three or more shells were available for comparison, increments prior to 1791 were not crossdated for this specimen; thus, the 427-year lifespan is a preliminary estimate. Nonetheless, this individual likely represents one of the longest-lived *A. islandica* specimens ever aged, approaching the lifespan of the longest-lived known specimen from North Iceland (507 years; Butler et al., 2013). Corrections made during crossdating (Table 3) were more often related to having measured false increments (n = 123) as opposed to having missed a measurement where increment boundaries are difficult to distinguish at first pass (n = 35). While such statistics are not usually reported with growth chronologies, they may provide indication of 1) the skill of the technician in accurately identifying growth increments at first pass, 2) the quality of the acetate peel or microscope image, and/or 3) the character of the shell itself indicating its tendency to exhibit false or difficult to distinguish annual growth lines due to environmental disturbance or other factors. Output from the ARSTAN and ShellCorr runs are provided as supplementary files.

3.2. Timing of the growing season of *A. islandica* from subannual $\delta^{18}O_{shell}$

The subannual $\delta^{18}O_{shell}$ values range from 1.26 ‰ to 3.05 ‰ with a standard deviation of 0.28 ‰ for micromilled samples. Eight samples were lost due to low sample size (i.e., loss of sample powder during transfer). For hand-drilled samples, $\delta^{18}O_{shell}$ values range from 2.02 ‰ to 2.97‰ with a standard deviation of 0.20 ‰. Two samples were lost due to low sample size (i.e., loss of sample powder during transfer) and one sample was excluded from further analysis as an outlier ($\delta^{18}O_{shell}$ = 3.34 ‰).

To determine the duration of the main growing season of *A. islandica*, reconstructed temperatures were placed along a temporal axis through aligning the individual series (taken over the years 2005–009) with the mean temperature at 100 m depth recorded at the FX3 and FX4 stations from 2002 to 2015 (Fig. 4) until the best visual agreement was achieved. For micromilled samples (where 10 samples were taken per annual increment), a mean series including three shells sampled over five years

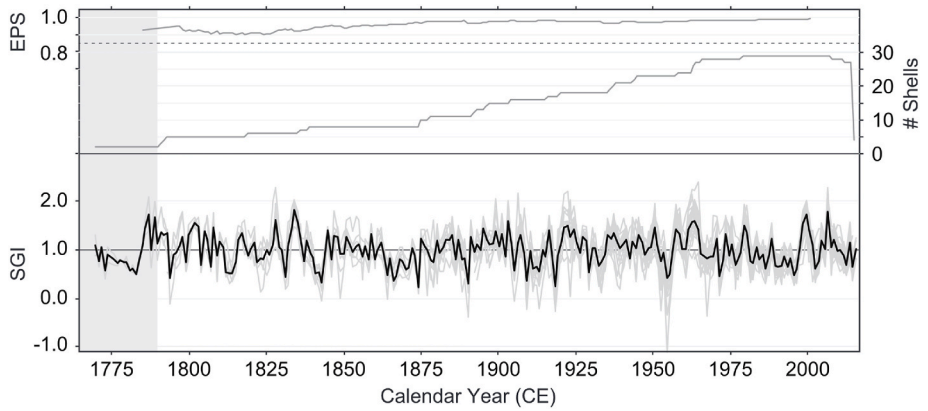

Fig. 3. SW Iceland shell growth chronology. (bottom, left axis) Individual detrended growth series (gray lines) and Master Shell Growth Chronology (MSC; black line) represented as shell growth indices (SGI), (middle; right axis) number of individual shell growth series included in the MSC, and (top, left axis) expressed population signal (EPS; solid line) and 0.85 EPS threshold (dashed line; see text). The shaded region prior to 1791 shows where the chronology contains fewer than 3 shells.

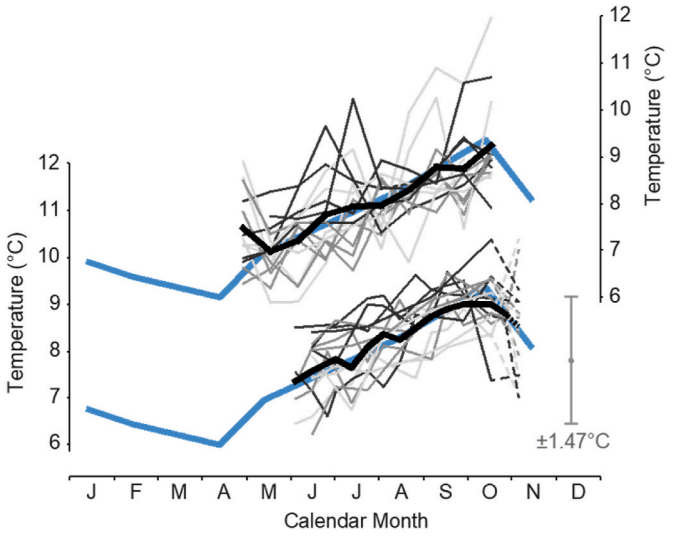

Fig. 4. Subannual $\delta^{18}O_{shell}$-based reconstructed temperature over five years (2005–2009) from three shells (gray lines) with mean across all samples (black) and instrumental temperature measurements from 100 m depth averaged between stations FX3 and FX4 from 2002 to 2015 (blue). Sampling was performed using a micromill (upper) and repeated by hand using a Dremel tool (lower). The dashed lines in the lower plot represent samples where shell was milled to include the material encompassing the increment line at the boundary of the annual growth increment (hand sampling). This is in contrast to sampling shell material deposited after (and not including) the increment line and up to the boundary (and not including) the following increment line (upper, micromill). The combined uncertainty (1.47 °C) is derived from uncertainty estimates related to instrumental precision (0.52 °C; 2 sigma standard deviation) and the Grossman and Ku (1986) temperature equation (1.37 °C; mean squared error). (For interpretation of the references to color in this figure legend, the reader is referred to the Web version of this article.)

was calculated by averaging data at each position along the growth increment (10 total across the growing season). For hand-drilled samples (where between 5 and 14 samples were taken per increment), data from annual increments having fewer samples (min n = 5) were spaced out evenly to align with the total number of data points from the annual increment having the greatest number samples (n = 14). The mean was then calculated at each position (14 total across the growing season). Visual alignment for the micromilled samples revealed an approximate shell-growing season commencing in May and ending through October. Because the hand-drilling technique included samples at the increment line (the boundary between years), incorporating material on both sides of the increment line, the final points in each of these series are considered shared between the previous and following growth increment (dashed lines in Fig. 4). With this consideration, the approximate growing season determined using both methods are in agreement.

3.3. Annual $\delta^{18}O_{shell}$ and reconstructed temperature

Annual $\delta^{18}O_{shell}$ values averaged across replicated years range from 2.21‰ to 3.34‰ with a standard deviation of 0.16‰ (hereafter, 1-sigma) and a mean of 2.67‰ (Fig. 5). Reconstructed temperatures from annual $\delta^{18}O_{shell}$, calculated using Equation (1), range from 5.6 °C to 9.5 °C with a mean of 7.5 °C (1765–2015 CE). The mean annual temperature reconstructed from $\delta^{18}O_{shell}$ (7.48 °C) compares well with the mean May–Oct temperature estimate from the loess-fit daily means of FX3 and FX4 data at 100 m depth (7.55 °C) and a mean May–Oct temperature time series of the FX3 and FX4 data filtered to years with at least two measurements available between May and October (7.21 °C; Fig. 6b).

3.4. Comparisons with other records

Correlations between the Faxaflói MSC and the North Icelandic shelf MSC (Butler et al., 2013), the northeast Iceland MSC (Lohmann and Schöne, 2013), the HadISST product, the AMV index, the NAO index, and the EA index revealed no significant relationships. The Faxaflói $\delta^{18}O_{shell}$ record shows weak yet significant negative correlation with the $\delta^{18}O_{shell}$ record from the North Icelandic Shelf ($r = -0.21$, $p < 0.01$, $n = 236$; Reynolds et al., 2016). Significant correlations were also found between the Faxaflói $\delta^{18}O_{shell}$ record and the winter (DJF) CPC NAO index ($r = -0.27$, $p < 0.05$, $n = 65$) and the annual (January–December) EA index ($r = -0.54$, $p < 0.001$, $n = 66$), but no significant correlation was found with the winter (DJF) EA index ($r = -0.13$, $p > 0.05$, $n = 66$). Correlations between the Faxaflói annual $\delta^{18}O_{shell}$ record and the annual (Jan–Dec) AMV index from van Oldenborgh et al. (2009) and Trenberth and Shea (2006) were insignificant, with $r = 0.10$ ($p > 0.05$, $n = 142$) and $r = 0.17$ ($p > 0.05$, $n = 127$), respectively.

The temperature reconstruction derived from $\delta^{18}O_{shell}$ (Fig. 6) exhibits weak but generally positive and significant correlations (Table 4) with annual (Jan–Dec) and growing season (May–Oct) SST products from nearby Faxaflói (HadISST; 64–65°N, 22–24°W) and instrumental records from nearby coastal monitoring stations (Reykjavík, Grindavík, and Stórhöfði/Vestmannaejar). Field correlation analysis (Fig. 7) reveals moderately positive and significant ($p < 0.05$) correlations between the reconstructed temperature and the HadISST gridded product (May–Oct) within Faxaflói as well as larger parts of the Nordic Seas and northern North Atlantic, excluding the subpolar gyre. Positive and significant correlations are maintained when series are detrended (not shown). Correlations between the temperature reconstruction and mean temperature time series at 100 m depth available from stations FX3 and FX4 (filtered to include years with more than two measurements available between May and October) are weakly positive but not significant.

4. Discussion

Temperature profiles within Faxaflói compiled from FX3 and FX4

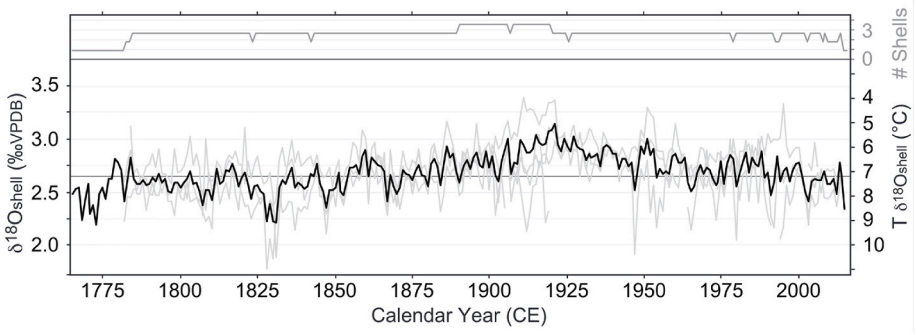

Fig. 5. SW Iceland $\delta^{18}O_{shell}$ chronology. Individual (gray) and mean (black) $\delta^{18}O_{shell}$ series (left axis) and equivalent temperature (right axis) assuming constant $\delta^{18}O_{water}$ of −0.07‰, and number of individual shell isotope series (top).

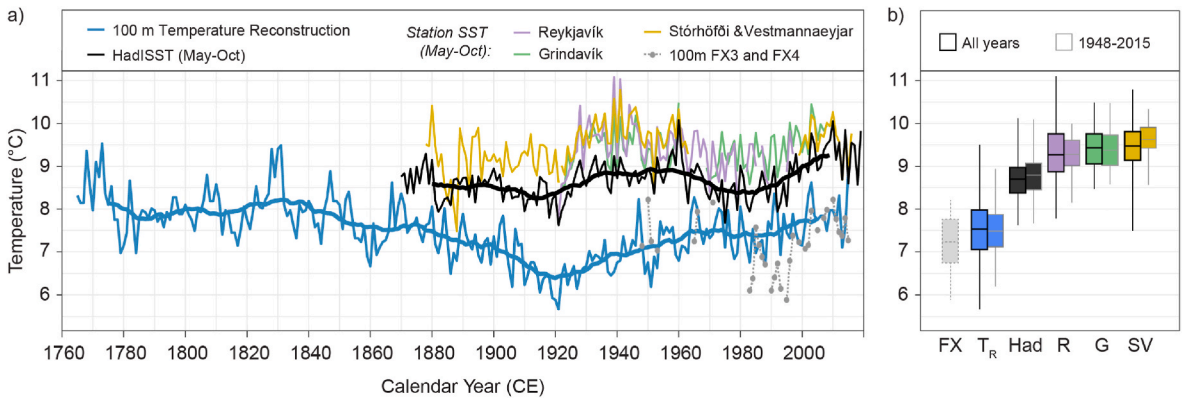

Fig. 6. Instrumental and reconstructed temperatures near Faxaflói. a) $\delta^{18}O_{shell}$-based temperature reconstruction (blue, T_R), May–October (growing season) local sea surface temperature measurements from monitoring stations near SW Iceland (purple, R = Reykjavík; yellow, SV = Stórhöfði/Vestmannaejar; green, G = Grindavík), May–October local sea surface temperature from the Hadley Centre gridded dataset (black, Had = HadISST, 22–24°W, 64–65°N), and May–October local temperatures measured at 100 m depth at stations FX3 and FX4 (gray, FX; filtered to only include years with at least two measurements between May and October). 21-year moving averages (thick lines) are shown for the reconstruction and HadISST series only. b) Box-and-whisker plots summarizing instrumental and reconstructed temperature series (whiskers extend to minimum and maximum, boxes extend to first and third quartiles, mean is noted by horizontal line). Summaries are shown for all available data (black outlines) and the period limited by available FX3 and FX4 data (gray outlines; 1948–2015). (For interpretation of the references to color in this figure legend, the reader is referred to the Web version of this article.)

Table 4
Pearson correlations coefficients (r) between $\delta^{18}O_{shell}$-temperature and local SST data. HadISST is taken from the region 22–24°W, 64–65°N encompassing Faxaflói. Correlations are also reported for linearly detrended data. Significant correlations ($p < 0.01$) are noted by asterisk, calculated based on r and degrees of freedom (d.f.; number of data pairs used in the comparison minus 1). Correlations were performed with FX3 and FX4 100 m May–Oct station data only for years with at least two FX measurements between May and October.

		detrended		detrended	
	Jan–Dec	Jan–Dec	May–Oct	May–Oct	d.f.
Reykyavík	0.09	0.25*	0.09	0.20	71
Grindavík	0.17	0.17	0.15	0.12	78
Stórhöfði/ Vestmannaejar	0.22	−0.09	0.19	0.06	103
HadISST	0.33*	0.26*	0.33*	0.26*	145
FX3 and FX4 100 m	n/a	n/a	0.20	.20	32

station records (Fig. 8) were useful in examining the timing of the growing season (Fig. 4) and revealing differences between the surface environment (0 m) and the bivalve habitat (100 m). The May–October growing season determined for the Faxaflói 100 m *A. islandica* population is in agreement with the population from the North Icelandic Shelf determined using similar methods (Reynolds et al., 2016). This time frame also marks the estimated average onset and breakdown of stratification in central Faxaflói (Fig. 8). The first major phytoplankton bloom in Faxaflói typically occurs at the onset of stratification near May, with secondary peak(s) occurring during mid-summer (Stefansson et al., 1987). Within Faxaflói, the mean temperature from May–Oct at 100 m depth from loess-filtered data compiled among stations FX3 and FX4 (7.55 °C) compares well with the mean annual reconstructed value (7.48 °C) during the period of overlap (1948–2015 CE).

Very few long-term, highly resolved instrumental temperature records are available from the marine environment below ~5-m depths by which to calibrate temperature reconstructions from proxy archives. The only instrumental dataset from 100 m depth with which to compare the

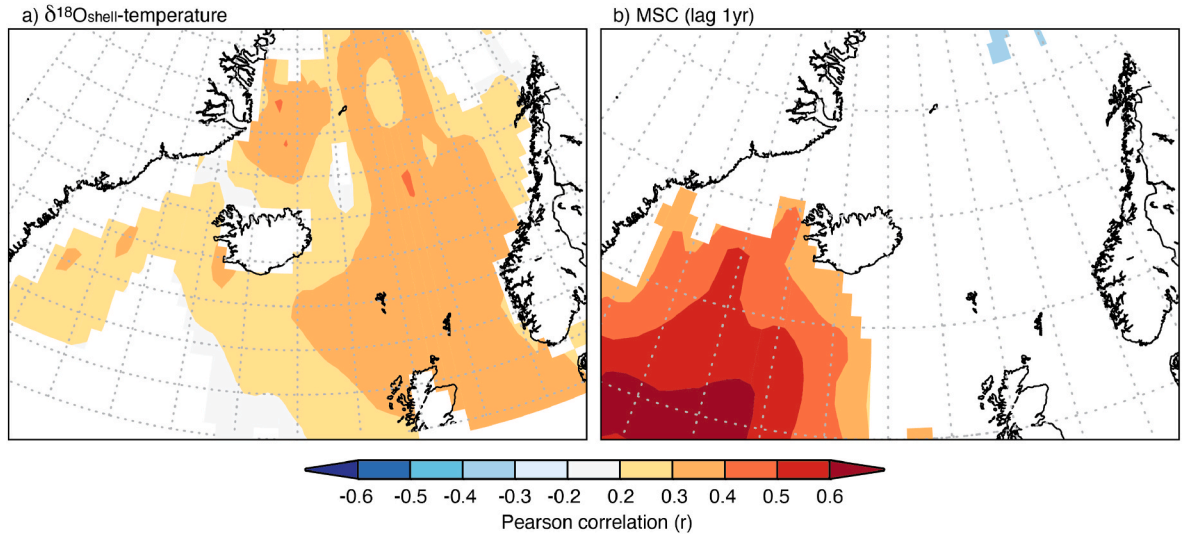

Fig. 7. Field correlation analysis between the annual $\delta^{18}O_{shell}$-temperature reconstruction (a; 1870–2015) and MSC lag-1yr (b; 1982–2015) with the HadISST gridded product. Correlations (color scale) are displayed where $p < 0.05$. Plots were produced using KNMI Climate Explorer (ps://climexp.knmi.nl/). (For interpretation of the references to color in this figure legend, the reader is referred to the Web version of this article.)

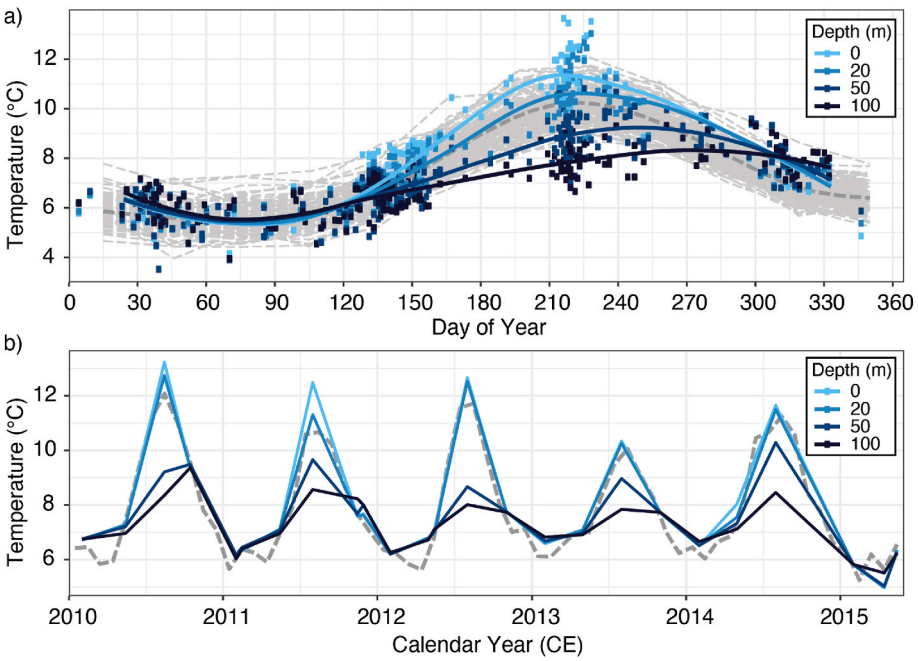

Fig. 8. Temperature records from stations FX3 and FX4 within Faxaflói and HadISST surface temperature records. a) Measurements compiled by day of year between 1947 and 2017 from 0 m, 20 m, 50 m, and 100 m depths at the FX3 and FX4 stations. Monthly HadISST are shown for comparison by individual years (thin dashed gray lines; centered on the 15th of each month) and mean across all years (bold dashed gray line) over the same time period. b) Timeseries of 0 m, 20 m, 50 m, and 100 m temperature at FX3 and FX4 (compiled as means over fortnightly periods) and monthly HadISST (bold dashed gray line) from 2010 to 2015.

temperature reconstruction is the sparsely sampled series compiled from stations FX3 and FX4. Most of these data were sampled in February, May, August, and November, with the majority (57%) of measurements made in months of the estimated growing season (May through October). However, annual means computed from these data are poor representations of seasonal or yearly averages and are difficult to interpret because only between one and nine (one to four) measurements are available in any given year for January through December (May through October). Correlations are weakly positive but not significant, likely in part due to this poor representation of annual (growing season) means. The average annual reconstructed temperature (7.48 °C), however, compares very well with May–Oct temperature estimated from the loess-fit daily means from FX3 and FX4 instrumental measurements at 100 m depth (7.55 °C). For comparison with a more complete annual time series, the $\delta^{18}O_{shell}$-temperature reconstruction was compared with a gridded SST product. The correlation between 0 m and 100 m temperature from the FX data of $r = 0.77$ ($p < 0.001$), highlights that while broad scale temperature trends are comparable in this region, the full character of deeper-water variability is not captured by surface waters. Therefore, we do not expect correlations between the $\delta^{18}O_{shell}$-temperature reconstruction from *A. islandica* at 100 m depth with SST records to exceed $r = 0.77$. The moderate positive correlations (Table 4) between the $\delta^{18}O_{shell}$-temperature reconstruction and the HadISST gridded product encompassing Faxaflói ($r = 0.26–0.33$) and nearest station-based SST record from Reykjavík ($r = 0.09–0.25$) are therefore supported. Correlations with other nearby station SST records were not as strong, likely due to increasing distance outside of Faxaflói. The positive correlations with available instrumental records analyzed here support the $\delta^{18}O_{shell}$-temperature reconstruction as the best available proxy indicator of water temperature variability at 100 m depth within Faxaflói. Further, annual (year-to-year) mean salinity at 100 m depth within Faxaflói varies minimally from year to year (2 sigma standard deviation = 0.11) with no clear seasonal cycle. Thus, we expect little influence from $\delta^{18}O_{water}$ (related to salinity) on $\delta^{18}O_{shell}$ and the resulting temperature reconstruction, however, long-term changes in $\delta^{18}O_{water}$ cannot be completely ruled out and remains an uncertainty in our reconstruction.

The field correlation analysis (Fig. 7) reveals coherence between the $\delta^{18}O_{shell}$-based temperatures and SST variability along the approximate path of North Atlantic waters approaching Iceland via the Irminger Current (Fig. 1), which represents more open ocean conditions. However, the same analysis identifies less coherence between the Faxaflói $\delta^{18}O_{shell}$-based temperatures and SST north of Iceland, likely reflecting the greater influence there of polar waters carried to the north Iceland area via the East Greenland and East Icelandic Currents. Further, the *A. islandica* $\delta^{18}O_{shell}$ records from Faxaflói and North Icelandic Shelf are inversely linearly related ($r = -0.21$, $p < 0.01$). Field correlations presented in Reynolds et al. (2016) identify high correlations between the North Icelandic Shelf $\delta^{18}O_{shell}$ record at 80 m depth with May–Oct SST and sea surface salinity in the region of the East Greenland and East Atlantic Currents (see Fig. 3 of Reynolds et al., 2016). The Faxaflói $\delta^{18}O_{shell}$-temperature reconstruction and the North Icelandic Shelf $\delta^{18}O_{shell}$ record, therefore both appear to reflect marine conditions of their respective regions, without sharing much common variance between them. The Faxaflói $\delta^{18}O_{shell}$-temperature reconstruction provides a strong indicator for variability of Atlantic Water entering the region via the Irminger Current prior to further transformation through mixing with the Icelandic Coastal Current and East Icelandic Current as it continues north and east along Iceland.

While *A. islandica* shell growth (MSC) in Faxaflói showed no significant year-to-year correlations with local instrumental temperature records, the significant positive correlation with HadISST across the subpolar gyre region when the MSC is lagged by 1 year (Fig. 7b) is mechanistically plausible. Other work identifies a similar leading relationship between subpolar gyre dynamics and zooplankton abundance on the Iceland shelf (Hátún et al., 2016). Food quality and quantity are known to be important factors controlling shell growth in *A. islandica* (Ballesta-Artero et al., 2018), thus we suspect the MSC–subpolar gyre SST relationship reflects effects of subpolar gyre dynamics on primary and secondary productivity propagated to the benthic community in Faxaflói, reflected as the 1-year lag in our shell growth index (Butler et al., 2013; Lohmann and Schöne, 2013; Carroll et al., 2014). The

MSC-subpolar gyre SST relationship is only evident when comparing with modern, satellite-derived datasets (post-1982), however, which might suggest environmental forcing from subpolar gyre dynamics plays an increasing role in driving Faxaflói ecosystem variability in recent decades. The lack of significant correlations found among MSCs between Faxaflói, the North Icelandic Shelf (Butler et al., 2013), and northeast Iceland (Lohmann and Schöne, 2013) suggests that these regions experience differing patterns of environmental variability, and possibly controls, on the rate of shell growth. Individually, none of these MSCs were correlated with gridded SST products at lag = 0, but correlations at varying time lags were either insignificant or not explored in these earlier works, and we find no significant correlations when repeating our lagged analysis between these MSCs and gridded SST products. Further investigation into the complex role of food and temperature variability on shell growth related to subpolar gyre dynamics and other local environmental forcings is thus warranted, and a potential direction for future work.

Correlations between the shell-based records and climate indices, including the AMV, NAO, and EA, were generally weak and insignificant. The NAO index describes the bipole contrast between a centre of high atmospheric pressure generally located near the Azores and a centre of low atmospheric pressure near Iceland. A positive NAO phase is associated with northward-shifted storm tracks and a stronger Atlantic jet stream (Hurrell, 1995). The paradigm model of the NAO's influence on ocean properties would predict cooler SSTs during positive NAO phases in this region (Visbeck et al., 2002), which is inconsistent with the significant negative correlation found between $\delta^{18}O_{shell}$ values and the winter NAO (and thus, positive correlation between reconstructed temperatures and NAO). Indeed, many studies identify such paradigm relationships as unstable through time or inconsistent at varying frequencies (Polyakova et al., 2006; Kenigson et al., 2018). Further, strongest NAO forcing occurs in the winter season, during which bivalve shell growth is extremely slow, and the NAO's influence on deeper water properties has not been well studied, limiting understanding of the expected influence of the winter NAO on shell growth. The EA, characterized by the second dominant mode of summer low-frequency variability in the Euro-Atlantic region, is known to influence the configuration of the NAO (intensity and locations of centers of action) and its impacts (Moore and Renfrew, 2012). A strong and significant negative correlation was found between $\delta^{18}O_{shell}$ and the annual (Jan–Dec) EA index ($r = -0.54$), but not with the winter EA index ($r = -0.13$), the latter of which is considered to be more relevant to associated climate variability and NAO behavior (Comas-Bru and McDermott, 2014). Finally, the AMV, which describes basin-scale sea surface temperature variability of the North Atlantic, is also not well reflected by the Faxaflói shell-based records. No significant correlations were found, even when shell-based records were smoothed to better match the smoothed nature (i.e., spatial-averaging) of the AMV indices. However, it is worth noting that the $\delta^{18}O_{shell}$-based temperatures (Fig. 6) exhibit an abrupt change from negative to positive trends around 1920, concurrent with a sharp increase in the AMV index at the onset of the Early Twentieth Century Warming of the 1920s–30s that engulfed the Atlantic Arctic (e.g.,Wood and Overland, 2010 and references therein). The weak, and somewhat inconsistent, correlations between shell-based records from Faxaflói and climate indices analyzed here are difficult to evaluate due to limited available research on the mechanistic relationships between these known climate modes and impacts on subsurface water properties, especially within Faxaflói. Further, the semi-enclosed nature of Faxaflói may impart more complex stratification and mixing dynamics that mask relationships larger-scale climate patterns and modes. Our results suggest more comprehensive analysis may be required to understand the complexities and expressions of larger-scale climate modes in this region.

5. Summary and conclusions

This study presents a 225-year crossdated master shell growth chronology (1791–2015 CE) and 251-year annual $\delta^{18}O_{shell}$ record (1765–2015 CE) from *A. islandica* bivalves in Faxaflói, Iceland. While shell growth rate, as represented by the MSC, was not correlated with available environmental records, a strong common growth signal is present, providing a robust chronology for the $\delta^{18}O_{shell}$-based temperature reconstruction. The MSC from Faxaflói shows no relationship with the North Icelandic Shelf or northeast Iceland MSCs, highlighting the spatial scale at which shell growth is synchronous among populations is exceeded in this case (Butler et al., 2009), and that shell growth among each location is driven by differing local patterns of environmental variability. Shell growth does, however, significantly correlate with SSTs across the subpolar gyre region at a lag of 1 year (SST leading shell growth) in recent decades. This finding provides direction for further investigation of these records and the influence of subpolar gyre dynamics on ecological indicators in southwest Iceland.

We provide an annually-resolved, absolutely-dated temperature reconstruction from a marine archive in the southwest Iceland region (Faxaflói). The $\delta^{18}O_{shell}$-temperature reconstruction from *A. islandica* shells collected at 100 m depth exhibits weak but significant relationships with the nearby marine surface temperature record at Reykjavík and a local gridded SST product (HadISST; 22–24°W, 64–65°N). The mean reconstructed temperature compares closely with available instrumental data from 100 m depth measured near the collection sites (1948–2015 CE), and is likely not significantly influenced by salinity (and $\delta^{18}O_w$) variation; however, long-term changes in $\delta^{18}O_{water}$ cannot be completely ruled out and remains an uncertainty in our reconstruction. The Faxaflói $\delta^{18}O_{shell}$ record shows a significant, yet inverse, relationship with the $\delta^{18}O_{shell}$ record from the North Icelandic Shelf comprising shells collected at ~82 m depth using similar methods (Butler et al., 2013; Reynolds et al., 2016). This may suggest that the added influence of polar waters entrained into the system to the north introduces structural changes in the organization of water masses around Iceland.

The newly constructed shell-based records provide a foundation for future work on *A. islandica* in southwest Iceland. Future studies could more thoroughly explore the relationships between deeper water dynamics in the Faxaflói region with subpolar gyre and other major circulation features to establish which aspects of larger-scale processes may be influencing deeper water benthic organisms. Comparisons with shallower-water populations may bring light to the strengths and limitations of *A. islandica* shell-based records in a semi-enclosed bay environment. Analysis of extreme events detected by the shell-based records may reveal further utility of the proxies in understanding or inferring large scale modes of variability and rapid climate changes. Additional studies could also utilize other proxy variables attainable from shell material, for example, radiocarbon or nitrogen isotopes as indicators of circulation changes through time.

Open research

The 225-year master shell growth chronology, 251-year $\delta^{18}O_{shell}$ record, and associated metadata are publicly available at https://www.ncei.noaa.gov/access/paleo-search/study/37020. Physical shell samples are stored at NORCE Norwegian Research Centre and are available upon request to C. Andersson (caan@norceresearch.no). Details on instrumental data and proxy-based records from other studies used for comparison can be found in the Methods section 2.4.

CRediT authorship contribution statement

M.J. Mette: Writing – original draft, Visualization, Methodology, Investigation, Formal analysis, Data curation. **C. Andersson:** Writing – review & editing, Supervision, Project administration, Investigation,

Funding acquisition, Data curation, Conceptualization. **B.R. Schöne:** Writing – review & editing, Resources, Investigation, Data curation. **F.G. W. Bonitz:** Writing – review & editing, Methodology, Investigation, Formal analysis, Data curation. **V. Melvik:** Methodology, Investigation, Formal analysis, Data curation. **T. Trofimova:** Writing – review & editing, Validation, Investigation. **M.W. Miles:** Writing – review & editing, Supervision, Project administration, Methodology, Investigation, Funding acquisition, Conceptualization.

Declaration of competing interest

The authors declare the following financial interests/personal relationships which may be considered as potential competing interests: Madelyn Mette has patent #5521421439016 licensed to John Wiley and Sons.

Data availability

Data will be made available on request.

Acknowledgments

The authors thank two anonymous reviewers and Alan Wanamaker for their time and valuable feedback. Any use of trade, firm, or product names is for descriptive purposes only and does not imply endorsement by the U.S. Government. This research was supported by the European Research Council under the European Community's Seventh Framework Programme (FP7/2007–2013)/ERC grant agreement 610055 ("the *ice2ice*" project), by the Icelandic Research Fund (RANNIS) grant 173906–051, and by the Norwegian Research Council grant 263053 ("ULTRAMAR" project). We thank Markus Reutter and Lisa Brombacher for obtaining water samples while studying at the University of Reykjavík (Erasmus student exchange program).

Appendix A. Supplementary data

Supplementary data to this article can be found online at https://doi.org/10.1016/j.ecss.2023.108525.

References

Ballesta-Artero, I., Janssen, R., van der Meer, J., Witbaard, R., 2018. Interactive effects of temperature and food availability on the growth of *Arctica islandica* (Bivalvia) juveniles. Mar. Environ. Res. 133 (November 2017), 67–77. https://doi.org/10.1016/j.marenvres.2017.12.004.

Black, B.A., Andersson, C., Butler, P.G., Carroll, M.L., DeLong, K.L., Reynolds, D.J., et al., 2019. The revolution of crossdating in marine palaeoecology and palaeoclimatology. Biol. Lett. 15 (1) https://doi.org/10.1098/rsbl.2018.0665.

Butler, P., Richardson, C., Scourse, J., Witbaard, R., Schöne, B., Fraser, N., et al., 2009. Accurate increment identification and the spatial extent of the common signal in five *Arctica islandica* chronologies from the Fladen Ground, northern North Sea. Paleoceanography 24. https://doi.org/10.1029/2008PA001715.

Butler, P., Richardson, C., Scourse, J., Wanamaker, A., Shammon, T., Bennell, J., 2010. Marine climate in the Irish Sea: analysis of a 489-year marine master chronology derived from growth increments in the shell of the clam Arctica islandica. Quat. Sci. Rev. 29, 1614–1632. https://doi.org/10.1016/j.quascirev.2009.07.010.

Butler, P., Wanamaker, A., Scourse, J., Richardson, C., Reynolds, D., 2013. Variability of marine climate on the North Icelandic Shelf in a 1357-year proxy archive based on growth increments in the bivalve *Arctica islandica*. Palaeogeogr. Palaeoclimatol. Palaeoecol. 373, 141–151. https://doi.org/10.1016/j.palaeo.2012.01.016.

Caesar, L., McCarthy, G.D., Thornalley, D.J.R., Cahill, N., Rahmstorf, S., 2021. Current atlantic meridional overturning circulation weakest in last millennium. Nat. Geosci. 14 (3), 118–120. https://doi.org/10.1038/s41561-021-00699-z.

Carroll, M., Ambrose, Locke, V, Ryan, S., Johnson, B., 2014. Bivalve growth rate and isotopic variability across the Barents Sea Polar. Front. J. Mar. Sys. 130, 167–180. https://doi.org/10.1016/j.jmarsys.2013.10.006.

Comas-Bru, L., McDermott, F., 2014. Impacts of the EA and SCA patterns on the European twentieth century NAO–winter climate relationship. Q. J. R. Meteorol. Soc. 140 (679), 354–363. https://doi.org/10.1002/qj.2158.

Cook, E., 1985. A Time-Series Analysis Approach to Tree-Ring Standardization. University of Arizona, Tuscon, AZ.

Cook, E.R., Peters, K., 1997. Calculating unbiased tree-ring indices for the study of climatic and environmental change. Holocene 7, 361–370.

Cook, E.R., Krusic, P.J., Peters, K., Holmes, R.L., 2017. Program ARSTAN (Version44), Autoregressive Tree–Ring Standardization Program. Tree–Ring Laboratory of Lamont–Doherty Earth Observatory.

Dettman, D., Reische, A., Lohmann, K., 1999. Controls on the stable isotope composition of seasonal growth bands in aragonitic fresh-water bivalves (unionidae). Geochem. Cosmochim. Acta 63 (7), 1049–1057. https://doi.org/10.1016/S0016-7037(99)00020-4.

Epstein, S., Buchsbaum, R., Lowenstam, H., Urey, H., 1953. Revised carbonate-water isotopic temperature scale. Geol. Soc. Am. Bull. 64 (11), 1315–1326. https://doi.org/10.1130/0016-7606(1953)64[1315:RCITS]2.0.CO, 2.

Fang, K., Gou, X., Peters, K., Li, J., Zhang, F., 2010. Removing biological trends from tree-ring series: testing modified Hugershoff curves. Tree-Ring Res. 66 (1), 51–59. https://doi.org/10.3959/2008-18.1.

Füllenbach, C.S., Schöne, B.R., 2015. Strontium/lithium ratio in shells of *Cerastoderma edule* (Bivalvia) – A new potential temperature proxy for brackish environments. Chem. Geol. 417, 341–355. https://doi.org/10.1016/j.chemgeo.2015.10.030.

Grossman, E., Ku, T.-L., 1986. Oxygen and carbon isotope fractionation in biogenic aragonite: temperature effects. Chem. Geol. 59, 59–74. https://doi.org/10.1016/0168-9622(86)90057-6.

Hátún, H., Lohmann, K., Matei, D., Jungclaus, J.H., Pacariz, S., Bersch, M., et al., 2016. An inflated subpolar gyre blows life toward the northeastern Atlantic. Prog. Oceanogr. 147, 49–66. https://doi.org/10.1016/j.pocean.2016.07.009.

Hurrell, J.W., 1995. Decadal trends in the North atlantic oscillation: regional temperatures and precipitation. Science 269, 67–69. https://doi.org/10.1126/science.269.5224.676.

Jones, P.D., Jonsson, T., Wheeler, D., 1997. Extension to the North Atlantic Oscillation using early instrumental pressure observations from Gibraltar and south-west Iceland. Int. J. Climatol. 17, 1433–1450. https://doi.org/10.1002/(SICI)1097-0088(19971115)17:13%3C1433::AID-JOC203%3E3.0.CO, 2-P.

Jónsson, T., 2003. Langtímasveiflur III. Sjávarhiti (Long-term sea-surface temperature measurements in Iceland). Icelandic Met. Office 1–15. VÍ-03013 (ÚR13) 15pp [in Icelandic]. https://www.vedur.is/media/vedurstofan/utgafa/greinargerdir/2003/03013.pdf.

Kenigson, J.S., Han, W., Rajagopalan, B., Yanto, Jasinski, M., 2018. Decadal shift of NAO-linked interannual sea level variability along the U.S. Northeast coast. J. Clim. 31 (13), 4981–4989. https://doi.org/10.1175/JCLI-D-17-0403.1.

Lohmann, G., Schöne, B., 2013. Climate signatures on decadal to interdecadal time scales as obtained from mollusk shells (*Arctica islandica*) from Iceland. Palaeogeogr. Palaeoclimatol. Palaeoecol. 373, 152–162. https://doi.org/10.1016/j.palaeo.2012.08.006.

Lund, D.C., Lynch-Stieglitz, J., Curry, W.B., 2006. Gulf Stream density structure and transport during the past millennium. Nature 444 (7119), 601–604. https://doi.org/10.1038/nature05277.

Marali, S., Schöne, B.R., 2015. Oceanographic control on shell growth of *Arctica islandica* (Bivalvia) in surface waters of Northeast Iceland - implications for paleoclimate reconstructions. Palaeogeogr. Palaeoclimatol. Palaeoecol. 420, 138–149. https://doi.org/10.1016/j.palaeo.2014.12.016.

Mette, M., Whitney, N., Ballew, J., Wanamaker, A.D., 2018. Unexpected isotopic variability in biogenic aragonite: a user issue or proxy problem? Chem. Geol. 483, 286–294. https://doi.org/10.1016/j.chemgeo.2018.02.027.

Mette, M., Wanamaker, A.D., Retelle, M.J., Carroll, M.L., Andersson, C., Ambrose, W.G., 2021. Persistent multidecadal variability since the 15th century in the southern Barents Sea derived from annually resolved shell-based records. J. Geophys. Res.: Oceans 126. https://doi.org/10.1029/2020JC017074.

Moffa-Sánchez, P., Moreno-Chamarro, E., Reynolds, D.J., Ortega, P., Cunningham, L., Swingedouw, D., et al., 2019. Variability in the northern North Atlantic and arctic oceans across the last two millennia: a review. Paleoceanogr. Paleoclimatol. 34 (8), 1399–1436. https://doi.org/10.1029/2018PA003508.

Moore, G.W.K., Renfrew, I.A., 2012. Cold European winters: interplay between the NAO and the East Atlantic mode. Atmos. Sci. Lett. 13, 1–8. https://doi.org/10.1002/asl.356.

Polyakova, E., Journel, A., Polyakov, I., Bhatt, U., 2006. Changing relationship between the North atlantic oscillation and key North Atlantic climate parameters. Geophys. Res. Lett. 33, 2–5. https://doi.org/10.1029/2005GL024573.

Rayner, N., Parker, D., Horton, E., Folland, C., Alexander, L., Rowell, D., et al., 2003. Global analyses of sea surface temperature, sea ice, and night marine air temperature since the late Nineteenth Century. J. Geophys. Res. 108 (D14), 4407. https://doi.org/10.1029/2002JD002670.

Reynolds, D.J., Scourse, J.D., Halloran, P.R., Nederbragt, A.J., Wanamaker, A.D., Butler, P.G., et al., 2016. Annually resolved North Atlantic marine climate over the last millennium. Nat. Commun. 7, 13502 https://doi.org/10.1038/ncomms13502.

Reynolds, D.J., Hall, I.R., Slater, S.M., Mette, M.J., Wanamaker, A.D., Scourse, J.D., et al., 2018. Isolating and reconstructing key components of North Atlantic Ocean variability from a sclerochronological spatial network. Paleoceanogr. Paleoclimatol. 33 (10), 1086–1098. https://doi.org/10.1029/2018pa003366.

Schöne, B., 2013. *Arctica islandica* (Bivalvia): a unique paleoenvironmental archive of the northern North Atlantic Ocean. Global Planet. Change 111, 199–225. https://doi.org/10.1016/j.gloplacha.2013.09.013.

Scourse, J., Richardson, C., Forsythe, G., Harris, I., Heinemeier, J., Fraser, N., et al., 2006. First cross-matched floating chronology from the marine fossil record: data from growth lines of the long-lived bivalve mollusc *Arctica islandica*. Holocene 7, 967–974. https://doi.org/10.1177/0959683606hl987rp.

Speer, J., 2010. Fundamentals of Tree-Ring Research. The University of Arizona Press, Tucson, AZ.

Stefansson, U., Thordardottir, T., Olafsson, J., 1987. Comparison of seasonal oxygen cycles and primary production in the Faxaflói region, southwest Iceland. Deep-sea Research I 34, 725–739. https://doi.org/10.1016/0198-0149(87)90033-1, 1987.

Trenberth, K.E., Shea, D.J., 2006. Atlantic hurricanes and natural variability in 2005. Geophys. Res. Lett. 33 (12), 1–4. https://doi.org/10.1029/2006GL026894.

van Oldenborgh, G., te Raa, L., Dijkstra, H., Philip, S., 2009. Frequency- or amplitude-dependent effects of the Atlantic meridional overturning on the tropical Pacific Ocean. Ocean Sci. 5 (3), 293–301. https://doi.org/10.5194/os-5-293-2009.

Visbeck, M., Chassignet, E.P., Curry, R., Delworth, T., Dickson, B., Krahmann, G., 2002. The ocean's response to North Atlantic Oscillation variability. In: The North Atlantic Oscillation: Climatic Significance and Environmental Impact, Geophysical Monograph Series. AGU, Washington, D. C, pp. 113–145, 134,.

Wanamaker, A., Butler, P., Scourse, J., Heinemeier, J., Eiríksson, J., Knudsen, K.L., Richardson, C., 2012. Surface changes in the North Atlantic meridional overturning circulation during the last millennium. Nat. Commun. 3 (899) https://doi.org/10.1038/ncomms1901.

Weidman, C., Jones, G., 1994. The long-lived mollusc *Arctica islandica*: a new paleoceanographic tool for the reconstruction of bottom water temperatures of the northern North Atlantic Ocean. J. Geophys. Res. 99 (C9), 18305–18314. https://doi.org/10.1029/94JC01882.

Wigley, T., Briffa, K., Jones, P., 1984. On the average value of correlated time series, with applications in dendroclimatology and hydrometeorology. J. Clim. Appl. Meteorol. 23 https://doi.org/10.1175/1520-0450(1984)023%3C0201:OTAVOC%3E2.0.CO, 2.

Wood, K., Overland, J., 2010. Early twentieth century Arctic warming in retrospect. Int. J. Climatol. 30, 1269–1279. https://doi.org/10.1002/joc.1973.

Zhang, R., Sutton, R., Danabasoglu, G., Kwon, Y.O., Marsh, R., Yeager, S.G., et al., 2019. A review of the role of the atlantic meridional overturning circulation in atlantic multidecadal variability and associated climate impacts. Rev. Geophys. 57 (2), 316–375. https://doi.org/10.1029/2019RG000644.